Journal of CO2 Utilization 102 (2025) 103220

Contents lists available at ScienceDirect

Journal of CO2 Utilization

journal homepage: www.elsevier.com/locate/jcou

Paradigmatic demonstration of sonochemical carbon dioxide reduction proceeded over Cu-based catalysts

Dong Xia [a,b,c,1], Yi Qin [b,1], Yagya N. Regmi [c], Laurie A. King [c,*], James Kwan [b,*]

[a] School of Chemical Engineering and Pharmacy, Wuhan Institute of Technology, Wuhan 430205, China
[b] Department of Engineering Science, University of Oxford, Oxford OX1 3PJ, UK
[c] Manchester Fuel Cell Innovation Centre, Manchester Metropolitan University, Manchester M1 5GD, UK

ARTICLE INFO

Keywords:
Cu catalysts
CO_2 reduction
Cavitation
Sonochemistry
Syngas synthesis

ABSTRACT

Sonochemical carbon dioxide (CO_2) reduction represents a promising decarbonization technology. However, relevant studies regarding the usage of solid catalysts in sonochemical reactor are rare. Herein, we investigate four distinct highly nanostructured cuprous oxides and sulfides for sonochemical CO_2 reduction via ultrasound-induced cavitation. Specifically, we investigate Cu_2O cubes, Cu_7S_4/Cu_2O cubes, Cu_7S_4 cages and Cu_7S_4 sheets morphologies. Each nanostructure is found to produce CO and H_2 in various ratios ranging from 1.0 – 2.3. Through a systematic study, we investigate the role of different acoustic conditions on affecting CO_2 sonolysis, involving the measurements in CO_2-saturated H_2O, 5 %CO_2/Ar-saturated H_2O, N_2-saturated H_2O, 5 %CO_2/N_2-saturated H_2O and CO_2-saturated $KHCO_3$. We show that Cu_2O cubes have the highest CO_2-to-CO conversion (up to 4286.4 $\mu mol \cdot L^{-1} \cdot g^{-1} \cdot h^{-1}$) in 5 %$CO_2$/Ar-saturated H_2O. In addition, the as-synthesized Cu_2O cubes exhibited promising sonochemical stability, with CO and H_2 production rates stabilizing at around 890.3 $\mu mol \cdot L^{-1} \cdot g^{-1} \cdot h^{-1}$ and 966.9 $\mu mol \cdot L^{-1} \cdot g^{-1} \cdot h^{-1}$, respectively. Post sonochemical analysis indicated that the Cu_2O cubes maintain relatively high CO_2-to-CO conversion, as well as their morphology. This work provides the first proof-of-concept demonstration of using inexpensive Cu-based catalysts to enable low-carbon sonochemical CO_2 reduction.

1. Introduction

The depletion of fossil fuels alongside the accumulation of CO_2 in the atmosphere is currently leading to critical environmental issues such as global warming, ocean acidification, glacier melting, and extreme weather events [1–4]. To address these critical challenges, numerous different carbon capture and utilization technologies have been developed to convert atmospheric CO_2 into value-added products, chemicals and feedstocks [5–10]. Despite great progress, commercially available technologies for CO_2 reduction to produce fuels and chemicals remain in their infancy, motivating the scientific community to investigate alternative approaches to this conversion.

Sonochemistry has recently gained traction as an attractive approach to drive chemical transformations, such as the conversion of CO_2 into value-added chemicals and fuels [11–13]. It operates on the principle of ultrasound-induced bubble formation, growth and collapse (acoustic cavitation), driving extreme reaction conditions such as temperatures up to 5000 K and pressures up to 1000 bar which can last for a few microseconds [14–17]. These conditions lead to the production of reactive intermediates (e.g., H•, CH_2•, HO•) [11,18], followed by initiating chemical reactions [19,20]. However, the electricity-driven yet low-carbon sonochemical CO_2 reduction reaction has not been intensively explored compared to the significant efforts dedicated to electrochemical [21], photochemical [22], thermochemical [23], biochemical [24] and piezo-photocatalytic CO_2 valorization [25,26]. Taken examples of activity improvement or catalyst preparation for boosted piezo-photocatalytic CO_2 conversion, Bi et al [26]. created a dual-site of La^{3+} and Al^{3+} in $SrTiO_3$ via the ball-milling molten salt process, leading to the obtained catalyst showing considerably enhanced CO_2 reduction performance. Zhu et al. [25]. prepared Au nanoclusters modified red graphitic carbon nitride catalyst for piezo-photocatalytic CO_2 reduction, which exposed more active Au sites resulting in improved CO production.

Previous studies have demonstrated that acoustic cavitation can drive the conversion of CO_2 into hydrocarbons, however, such studies utilized catalyst-free systems and required multivariant gases (e.g. Ar,

* Corresponding authors.
E-mail addresses: l.king@mmu.ac.uk (L.A. King), james.kwan@eng.ox.ac.uk (J. Kwan).
[1] These authors contributed equally.

https://doi.org/10.1016/j.jcou.2025.103220
Received 11 July 2025; Received in revised form 21 August 2025; Accepted 11 September 2025
Available online 19 September 2025

He, N_2 or H_2) to activate efficient CO_2 sonolysis [27,28]. Higher solubility of CO_2 in a multivariant gas environment tends to promote bubble coalescence instead of inertially collapsing cavitation bubbles. Thus, CO_2 only saturated solutions generally have reduced sonochemical activity [19]. For example, Harada demonstrated CO_2-to-CO conversion in CO_2/Ar, CO_2/He, CO_2/H_2 or CO_2/N_2 atmospheres, whereas pure CO_2-saturated H_2O showed no evidence of CO_2 reduction [28]. Similarly, Islam et al. [27] found a dramatically lower sonochemical activity in pure CO_2-saturated H_2O compared to CO_2/H_2, CO_2/N_2, and CO_2/Ar saturated water. Notably, in this study, with the presence of H_2, hydrocarbons such as CH_4, C_2H_4 and C_2H_6 were detected. Gireesan et al. [13] adopted a diffusion limited model to simulate the collapse intensity of a single Ar-CO_2 bubble to develop fundamental insight regarding the concentration effect of dissolved CO_2 on cavitation. They observed that a higher proportion of CO_2 in the Ar/CO_2 bubble led to a significantly reduced collapse intensity, as characterized by decreased generation of radicals. In addition, a higher fraction of dissolved CO_2 resulted in enlarged bubble size containing higher water vapor concentration which resulted in a significantly decreased temperature upon collapse.

Recently, catalysts have been investigated for sonochemical CO_2 reduction. To date, such studies have demonstrated improved CO_2 reduction performance even in pure CO_2-saturated solutions (without multivariant gas environments) compared to catalyst-free sonochemical CO_2 reduction. For instance, Ma et al. [29] fabricated $H_2Ti_3O_7$ nanowires to conduct sonochemical CO_2 reduction for 2 h in CO_2-saturated H_2O containing sacrificial sodium sulfide and sodium sulfite, which demonstrated a marked CO production rate of 8.3 $\mu mol \cdot L^{-1} \cdot g^{-1} \cdot h^{-1}$. More recently, Babikir et al. [12] highlighted that cavitation events enabled conversion of CO_2 to multicarbon products of oxygenates (9 ppm of ethanol and 6 ppm of acetone) and acetamide (10 ppm) at 70 °C for 2 h, upon the utilization of liquid metal gallium catalysts in 20 mL CO_2-saturated H_2O containing 1 mL of NH_4OH solution. These investigations report excellent catalyst promoted CO_2 sono-reduction performance but the reported systems either needed the addition of sacrificial agents [29] or worked at an elevated temperature [12]. Evidently, the development of high-performing metal-based catalysts that can induce strong cavitation events on their own for CO_2 conversion is of crucial urgency and significance to fill in the gap [30].

Inspired by the high performance (activity, selectivity and durability) of Cu-based catalysts for electrochemical CO_2 reduction [5,31,32], herein we synthesized four Cu-based catalysts for sonochemical CO_2 reduction. Namely we prepared Cu_2O cubes, Cu_7S_4/Cu_2O cubes with a configuration of Cu_7S_4 nanosheet-shell encapsulating Cu_2O cores, Cu_7S_4 cages and Cu_7S_4 sheets. Among them, the Cu_2O cubes exhibited the most optimal CO_2-to-CO conversion in CO_2-saturated H_2O with 272.1 $\mu mol \cdot L^{-1}$ per gram catalyst ($\mu mol \cdot L^{-1} \cdot g^{-1}$) CO yield. In addition to CO, H_2 was also produced with a CO/H_2 ratio across all of the as-synthesized catalysts of 1.0 – 2.3 (syngas). The role of atmosphere on sonochemical CO_2 reduction performance was also investigated. We demonstrate that a dramatic sonochemical CO_2-to-CO conversion improvement was achieved, reaching 1428.8 $\mu mol \cdot L^{-1} \cdot g^{-1}$, equivalent to a CO production rate of 4286.4 $\mu mol \cdot L^{-1} \cdot g^{-1} \cdot h^{-1}$, upon using 5 % CO_2/Ar-saturated H_2O. To understand the durability of the Cu_2O cubes for sonochemical CO_2 reduction, long-term experiments were conducted. The Cu_2O cubes catalysts experienced only slight morphological deformation during the 40-minute test, with relatively small changes to the CO_2 reduction activity during CO_2 sonolysis. This work highlights the opportunity to develop various Cu-based catalysts for converting CO_2 into high-value chemicals via sonochemistry.

2. Materials synthesis

2.1. Catalyst synthesis

Cu-based catalysts were synthesized following literature protocols with slight modifications [33]. Specifically, the Cu_2O cubes were synthesized by dissolving $Cu(CH_3COO)_2$ (2.9946 g) in a beaker containing deionized H_2O (50 mL) at 70 °C with continuous stirring. Subsequently, 30 mL of 3 $mol \cdot L^{-1}$ NaOH was added to the beaker dropwise to produce dark precipitates, and the mixed solution stirred for a further 20 min. Glucose powder (0.6 g) was then added with constant stirring. The wet Cu_2O cubes precipitates were washed using deionized H_2O and ethanol and dried overnight at 60 °C to obtain the Cu_2O cubes. To synthesize the Cu_7S_4/Cu_2O cubes, 0.36 g Na_2S and 0.006 g NaOH were dissolved in 150 mL anhydrous ethanol solution, followed by adding 0.6 g of the obtained Cu_2O cubes catalysts to the as-prepared solution with a continuous stirring for 10 min. The resultant black precipitates were washed by deionized H_2O and ethanol, followed by centrifugation and drying at 60 °C. The Cu_7S_4 cages catalysts were synthesized by dispersing the obtained Cu_7S_4/Cu_2O cubes in $NH_3 \cdot H_2O$ solution (25 %) for 3 days to remove the Cu_2O core; centrifuging and washing with deionized water and anhydrous ethanol; and drying overnight at 60 °C. To produce the Cu_7S_4 sheets, 25 mL of *n*-propanol and 25 mL of deionized H_2O were added to the $NH_3 \cdot H_2O$ solution (25 %), followed by stirring and sonication. The precipitate was washed, centrifuged and dried as described above.

2.2. Materials characterization

X-ray diffraction (XRD) patterns were collected on the powder X-ray diffractometer (PANalytical X'pert) using Cu Kα source (λ = 1.5406 Å). Scanning electron microscopic (SEM) images were taken by a Zeiss Sigma 300 microscope (Oxford Instruments). Scanning electron microscope-energy dispersive X-ray (SEM-EDX) images were collected by the Zeiss Crossbeam 350 FIB-SEM (Zeiss Crossbeam). The particle size of as-synthesized catalysts was statistically analyzed by ImageJ. X-ray photoelectron spectroscopy (XPS) was collected at the Kratos Analytical (a Shimadzu group company), AXIS Supra+ . The collected XPS spectra were then calibrated based on the C 1 s spectrum at a binding energy of 284.8 eV.

2.3. Sonochemical CO_2 reduction

Sonochemical CO_2 reduction was performed in a customized cylindrical sonochemical reactor (Figure S1). Detailed information about the reactor is provided in a previous study [17]. In brief, an air-tight vial (5 mL PPE test tube) equipped with a syringe was used as the container to store 2.5 mL of liquid solution and 5 mg catalyst. Prior to CO_2 sonocatalysis, the reactor solution was saturated with gas (e.g., pure CO_2, 5 %CO_2/Ar, 5 %CO_2/N_2, or N_2) for 15 min. The samples were exposed to ultrasound followed by cavitation in the cylindrical sonochemical reactor for 20 min under peak to peak drive voltage of 251 V (parameters of KEYSIGHT 33600 A waveform generator: frequency of 1.076 MHz; cycle count of 100; and burst period of 1.000 ms). Post sonication, the reactor valve of the equipped syringe was switched on to draw the gases from the headspace to be analyzed by gas chromatography (Shimadzu GC-2030). Nuclear magnetic resonance (NMR) was utilized to detect liquid products (JEOL JNM-ECZR 500 MHz spectrometer). Specifically, the reaction mixtures were centrifugated to separate catalysts as precipitates, and the supernates (0.5 mL) mixed with 0.15 mL of D_2O and 0.1 mL of DMSO for NMR measurement. To assess the stability of the sonocatalysis, the experiment was extended for various time intervals (5 min, 10 min, 30 min and 40 min), with all other parameters unchanged as-described above. The detailed methods to calculate the yielded products and product yield rates are provided in the Supporting Information.

3. Results and discussion

3.1. Characterization of as-synthesized catalysts

To explore the efficacy of Cu-based catalysts for sonochemical CO_2

reduction, various nanostructured copper oxide and sulfide materials were synthesized. Specifically, Cu_2O cubes, Cu_7S_4 shell-Cu_2O cube core (abbreviated as Cu_7S_4/Cu_2O cubes), Cu_7S_4 cages and Cu_7S_4 sheets (Fig. 1a) were prepared following literature methods [33]. The morphologies and chemical compositions of the as-synthesized catalysts were confirmed by electron microscope imaging and energy dispersive X-ray spectroscopy (SEM-EDX) (Fig. 1b-e).

The crystal structures of the synthesized catalysts were assessed by XRD (Fig. 1h). Specifically, the as-synthesized Cu_2O cubes exhibit cubic morphologies with a roughened surface (Fig. 1b), with an average particle size of 827 ± 134 nm. The Cu_7S_4/Cu_2O cubes' surface is decorated with highly roughened Cu_7S_4 nanosheets which encapsulate the Cu_2O core (Fig. 1c), exhibiting an enlarged particle size of 1034 ± 128 nm. Cu_7S_4 cages (prepared by dissolution of the Cu_2O core) are hollow structures (Fig. 1d), with an averaged particle size of 943 ± 171 nm. Finally, the collapse of Cu_7S_4 cages results in the formation of smaller and agglomerated nanostructures compared to the other structure, featuring apparent agglomerated sheet morphology, thus denoted as Cu_7S_4 sheets for simplicity (Fig. 1e). The as-synthesized Cu_7S_4 sheets featured a single sheet size of 135 ± 26 nm (Figure S2). SEM-EDX mapping was conducted on the Cu_2O cubes and Cu_7S_4 sheets, to confirm the conversion of Cu_2O to Cu_7S_4. As expected, for all measured Cu_2O, a uniform distribution of Cu was observed (Fig. 1f). Similarly, a uniform Cu and S distribution was observed in the Cu_7S_4 sheets (Fig. 1g), confirming the formation of copper sulfide material (Fig. 1h).

To probe the crystallinity of the samples, XRD was performed. The diffraction pattern for Cu_2O cubes contain pronounced diffraction peaks of (110), (111), (200), (211), (220), (311) and (222) (PDF#05–0667 Cu_2O), indicating a Cu_2O cubic structure. In addition, a low intensity peak at 38.8° is observed and assigned to the (111) plane of CuO. XRD also verified the presence of Cu_7S_4 monoclinic structure in Cu_7S_4/Cu_2O cubes, Cu_7S_4 cages and Cu_7S_4 sheets. As to Cu_7S_4/Cu_2O cubes, only (040) and (304) (PDF#33–0489 Cu_7S_4) diffraction peaks of Cu_7S_4 were observed. Conversely, for both Cu_7S_4 cages and Cu_7S_4 sheets multiple diffraction peaks are observed, including (013), (022), (113), (004), (104), (031), (302) and (422) (PDF#33–0489 Cu_7S_4) .

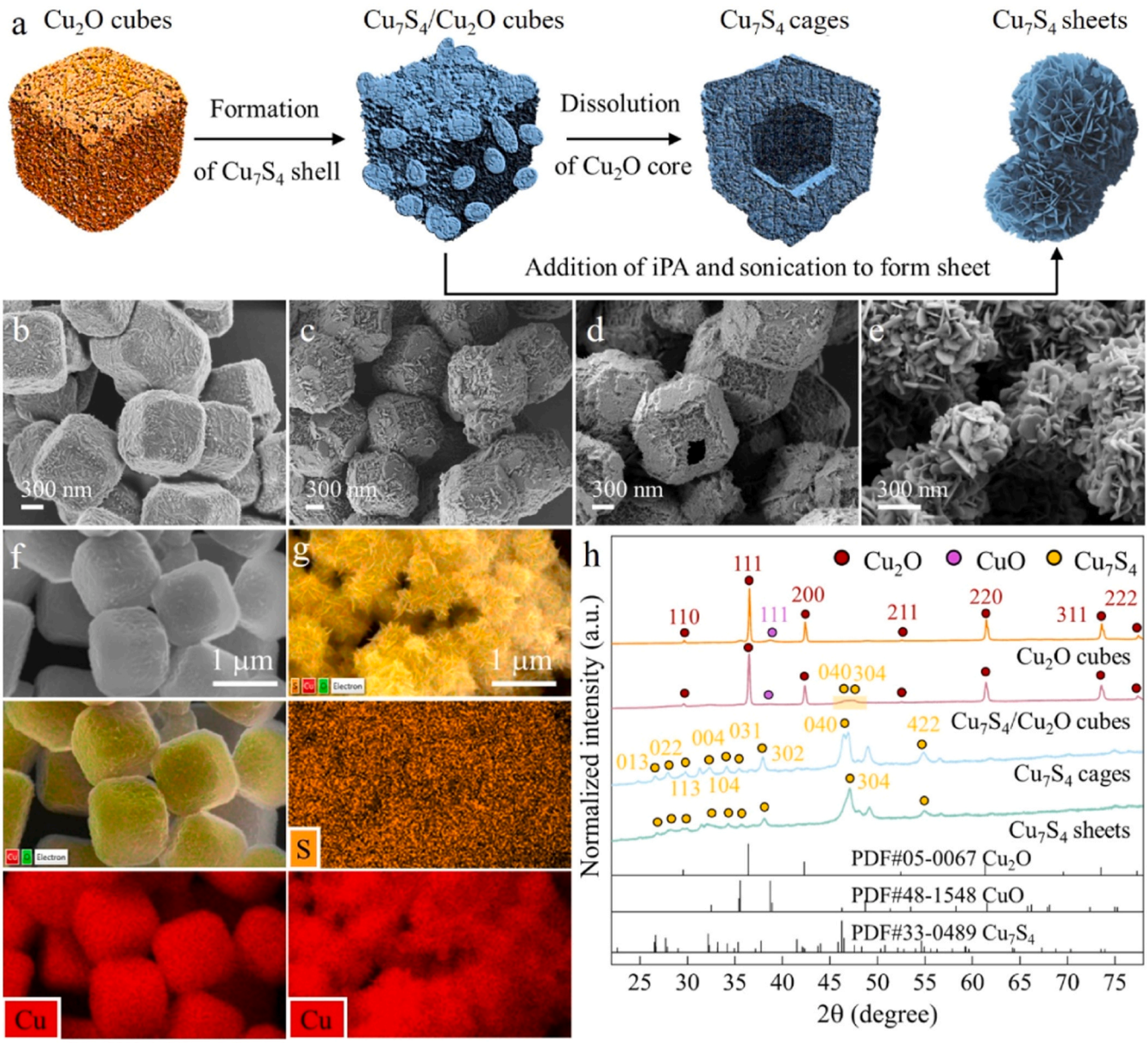

Fig. 1. (a) Schematic of the synthetic methods to prepare Cu_2O cubes, Cu_7S_4/Cu_2O cubes, Cu_7S_4 cages and Cu_7S_4 sheets. SEM images of Cu_2O cubes (b), Cu_7S_4/Cu_2O cubes (c), Cu_7S_4 cages, (d) and Cu_7S_4 sheets. (e) SEM-EDX mapping images of (f) Cu_2O cubes and (g) Cu_7S_4 sheets. (h) XRD patterns of the as-synthesized catalysts.

3.2. Evaluation of sonochemical CO_2 reduction

Sonochemical CO_2 reduction was performed in a gas-tight vial containing catalyst and various gas-saturated solutions. Prior to introducing the catalyst particles, a catalyst-free CO_2-saturated H_2O solution was first sonicated. No products were detected, confirming that any subsequent CO_2 conversion was dependent on the added catalysts. This was consistent with literature reports which have reported that highly soluble CO_2 causes increased bubble-bubble coalescence leading to highly suppressed sonochemical activity [11,27,34].

All four catalysts were shown to be active for sonochemical CO_2 reduction, producing CO and H_2 only under CO_2 saturated conditions (catalyst loading of 2 mg·mL^{-1}). Specifically, the Cu_2O cubes yielded 272 μmol·L^{-1}·g^{-1} of CO and 270.4 μmol·L^{-1}·g^{-1} of H_2, and the CO/H_2 ratio of was 1.0 (Fig. 2a). These observed results affirmed that the usage of Cu-based catalysts are able to significantly improve the sonochemical CO_2 reduction performance, unlike previously reported catalyst-free CO_2 sonolyis systems that required complex atmospheres to acquire effective CO_2 reduction sonocativity [11]. On top of the marked improvements in CO_2 reduction performance, the power input used in our customized cylindrical sonochemical reactor was only 20.2 W, which was substantially lower than the power of 77.8 W needed in previously reported CO_2 sonolysis system containing no catalysts [27].

The Cu_2O cubes exhibited the highest CO yields (272.1 μmol·L^{-1}·g^{-1}), followed by Cu_7S_4 sheets (177.4 μmol·L^{-1}·g^{-1}), Cu_7S_4/Cu_2O cubes (164.3 μmol·L^{-1}·g^{-1}) and Cu_7S_4 cages (101.8 μmol·L^{-1}·g^{-1}). The CO/H_2 ratio across all of the tested catalysts fell within the typical range for syngas (1.0, 1.6, 2.3 and 1.5 for Cu_2O cubes, Cu_7S_4/Cu_2O cubes, Cu_7S_4 cages and Cu_7S_4 sheets, respectively, Fig. 2b) [35–37]. As the CO/H_2 ratios range between 1.0 and 2.3, the sonochemically derived syngas can be used for the industrial Fischer-Tropsch processes that typically need a syngas with the CO/H_2 ratio spanning from 0.5 and 2.0 to manufacture high-value chemical compounds such as CH_4 and long-chain hydrocarbons [35–37]. Owing to the high energy of sonochemical processes which result in high temperatures (~5000 K) and pressures (~1000 bar), it is critical to investigate catalyst stability during sonolysis [38,39]. SEM was used to investigate the morphological integrity of catalysts (Fig. 1b-e, and Fig. 2b). Interestingly, the more active catalysts (Cu_2O cubes and Cu_7S_4 sheets) had only slight morphological deformation post sonolysis. Conversely, the two catalysts with lower activities (Cu_7S_4/Cu_2O cubes and Cu_7S_4 cages) displayed significant morphological deformations. Whisker-like structures develop at the surface post CO_2 reduction when comparing Fig. 1b and c with corresponding post sonolysis images in Fig. 2b (two images at the center). To assess the crystal structures of the catalysts as a function of sonolysis, XRD patterns of the spent catalysts were collected (Figure S3). No significant changes in XRD patterns were observed post sonolysis for the more active Cu_2O cubes and Cu_7S_4 sheets (Fig. 1d and Figure S3). In comparison, XRD patterns of the less active Cu_7S_4/Cu_2O cubes and Cu_7S_4 cages show distinctly apparent crystal structure evolution during CO_2 sonolysis (Fig. 1d and Figure S3). We therefore hypothesize that the morphological and crystallographic deformation in Cu_7S_4/Cu_2O cubes and Cu_7S_4 cages resulted in lower CO_2-to-CO conversion.

3.3. Performance optimization of sonochemical CO_2 reduction

To further improve the sonochemical CO_2 conversion performances via reaction condition optimizations, a broad spectrum of reaction conditions were investigated utilizing the two highest performance catalysts established through the initial screening (Cu_2O cubes and Cu_7S_4 sheets). Specifically, different concentrations of $KHCO_3$ solutions (0.1 M, 0.3 M and 0.5 M) and reaction atmospheres (e.g. 5 %CO_2/Ar,

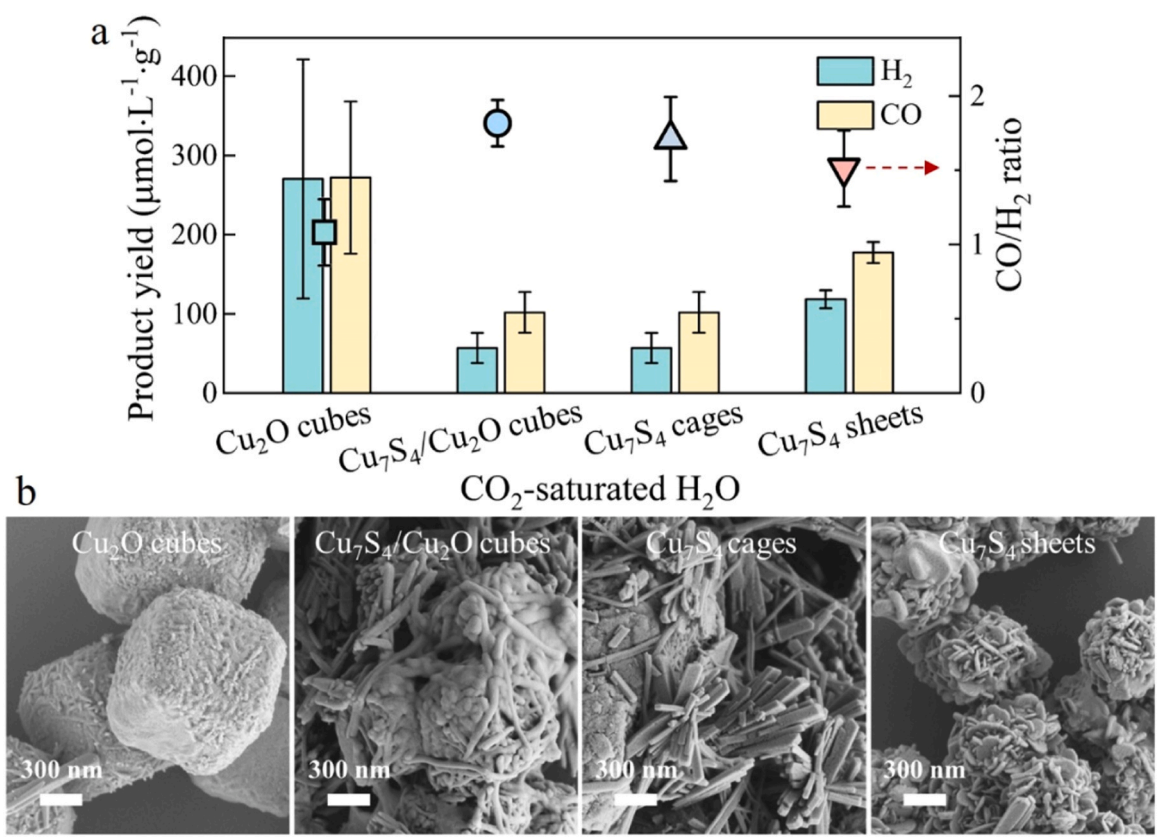

Fig. 2. (a) Product yields and measured CO/H_2 ratio in CO_2-saturated H_2O, for the four synthesized catalysts with a catalyst loading of 2 mg·mL^{-1} (Cu_2O cubes, Cu_7S_4/Cu_2O cubes, Cu_7S_4 cages and Cu_7S_4 sheets). (b) Corresponding SEM images of Cu_2O cubes, Cu_7S_4/Cu_2O cubes, Cu_7S_4 cages and Cu_7S_4 sheets after 20 min sonochemcial CO_2 reduction.

5 %CO_2/N_2 and N_2) were investigated. As shown in Fig. 3a, both Cu_2O cubes and Cu_7S_4 sheets demonstrate a lower CO_2-to-CO conversion rate in CO_2-saturated $KHCO_3$ solutions (regardless of concentrations) when compared to CO_2-saturated H_2O. The reduced CO_2-to-CO conversion performance in CO_2-saturated $KHCO_3$ solutions may be due to the increased CO_2 solubility and solution viscosity which likely leads to a reduced amount of inertial cavitation bubbles [27].

It is notable that Ar is commonly used in the literature to improve the chemical effects of cavitation. This is reportedly due to it being a monoatomic gas with a higher polytropic ratio (γ=1.66) and a lower thermal conductivity (λ=0.018 $W \cdot m^{-1} \cdot K^{-1}$) [27,40]. These properties boost inertial cavitation, increasing the temperature of the bubble during collapse, and in turn, lead to increased sonochemical activity [19]. As expected, the CO_2-to-CO conversion in 5 %CO_2/Ar-saturated H_2O further increased up to 1428.8 $\mu mol \cdot L^{-1} \cdot g^{-1}$ (Fig. 3a), which was more than five times higher than the CO_2-saturated H_2O (272.1 $\mu mol \cdot L^{-1} \cdot g^{-1}$). These results corroborate with previously reported catalyst-free system involving the usage of Ar to boost CO_2 sonolysis [28].

Under 5 %CO_2/N_2-saturated H_2O, no CO was observed with H_2 as the only product (Fig. 2b). This can be attributed to the lower polytropic ratio (γ=1.40) of N_2 and a higher thermal conductivity (λ= 0.024 $W \cdot m^{-1} \cdot K^{-1}$) compared to Ar [40]. As expected, no CO was produced in N_2-saturated H_2O reaction (Fig. 3a) because the reactant CO_2 was absent. However, the H_2 production performance improved considerably compared to Ar-free atmospheres, indicating that Cu_2O cubes catalysts can also be utilized for sonochemical H_2 production. Interestingly, 5 %CO_2/N_2-saturated H_2O (Fig. 3d) suppressed H_2 generation in comparison to 5 %CO_2/Ar-saturated H_2O and N_2-saturated H_2O, suggesting that the H_2 production rate can be controlled by changing the gaseous atmospheres upon using the Cu_2O cubes catalysts, further demonstrating the catalytic multifunctionality of the Cu_2O cubes catalysts.

To further understand the differences in CO_2-to-CO conversion as a function of reactor environments, the catalyst morphology and crystalline structure were characterized post-reaction by SEM and XRD. The highest performing catalyst (Cu_2O cubes) and reaction conditions (5 % CO_2/Ar-saturated and N_2-saturated H_2O conditions), demonstrates a stable morphology post sonolysis (Fig. 3c and Fig. 3e). In stark comparison, the CO_2-saturated $KHCO_3$ solutions (Figs. 3f-3h) caused significant morphological deformations of Cu_2O cubes compared to that of CO_2-saturated H_2O (Fig. 3b). Such morphological deformations likely contributed to the deterioration of CO_2-to-CO conversion (Fig. 3a). The preservation of the catalyst morphology and crystal structure provided additional evidence to underscore the importance of structural integrity for sonochemical CO_2 reduction, which aligned with the conclusions resulting from CO_2-saturated H_2O experiments discussed in the previous section. XRD (Figure S4) confirmed that the bulk Cu_2O crystallinity was retained for all reaction conditions, and only slight crystallite size changes were observed post sonolysis.

3.4. Evaluation of the stability of catalysts

Cu_2O cubes exhibited the highest CO_2-to-CO conversion performance in CO_2-saturated H_2O, and therefore its long-term operation was assessed. As presented in Fig. 4, the catalyst is shown to be active throughout the duration of the stability measurements, producing both CO and H_2. The quantity of CO and H_2 reached 605.1 $\mu mol \cdot L^{-1} \cdot g^{-1}$ and 685.3 $\mu mol \cdot L^{-1} \cdot g^{-1}$, respectively, within 40 min. Rates for production of CO and H_2 (890.3 $\mu mol \cdot L^{-1} \cdot g^{-1} \cdot h^{-1}$ and 966.9 $\mu mol \cdot L^{-1} \cdot g^{-1} \cdot h^{-1}$,

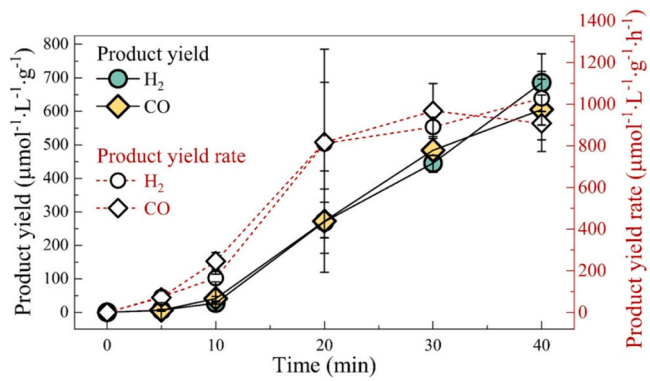

Fig. 4. Sonochemical stability testing of the Cu_2O cubes catalysts in CO_2-saturated H_2O.

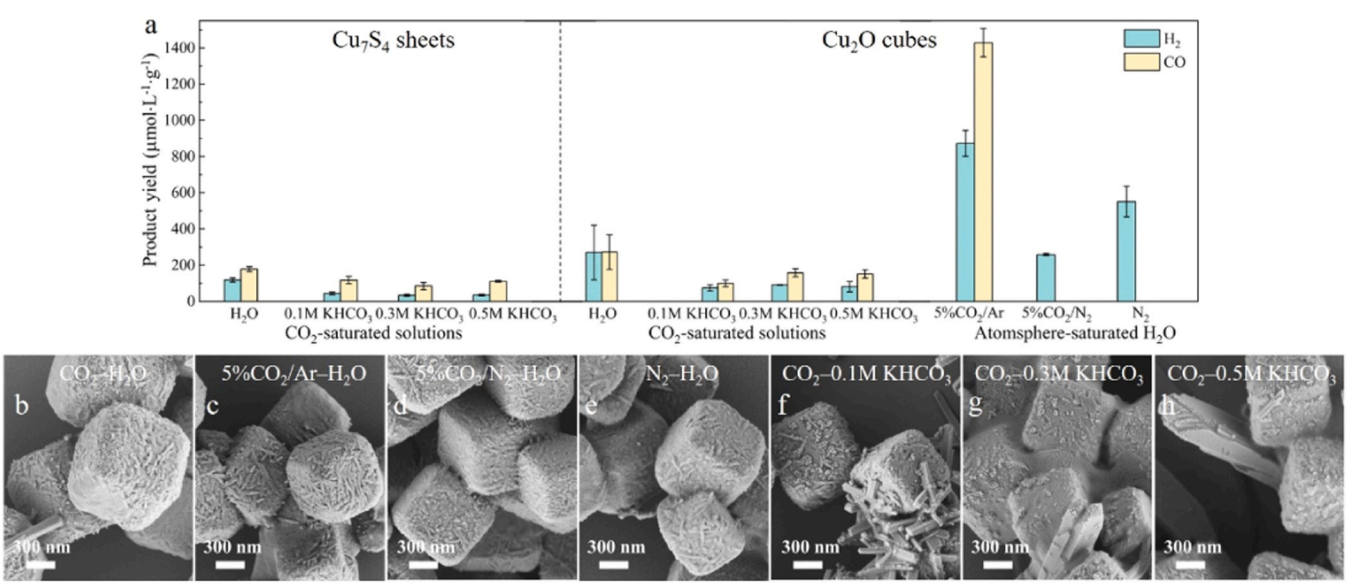

Fig. 3. (a) Product distribution analysis of sonochemical CO_2 reduction of Cu_2O cubes and Cu_7S_4 sheets operated in different reaction conditions, with the optimal Cu_2O cubes being additionally measured in 5 %CO_2/Ar-saturated H_2O, 5 %CO_2/N_2-saturated H_2O and N_2-saturated H_2O. Corresponding SEM images of Cu_2O cubes collected after sonochemical CO_2 reduction in various reaction conditions, including CO_2-saturated H_2O (b), 5 %CO_2/Ar-saturated H_2O (c), 5 %CO_2/N_2-saturated H_2O (d), N_2-saturated H_2O (e), CO_2-saturated 0.1 M $KHCO_3$ (f), CO_2-saturated 0.3 M $KHCO_3$ (g) and CO_2-saturated 0.5 M $KHCO_3$ solutions (h).

respectively) reached equilibrium after 30 min of operation. The average CO/H_2 ratio was 0.9 which is again within the accepted range for syngas.

To assess the Cu_2O cubes' stability as a function of time, the morphology, crystallinity and composition were characterized after 20 mins reaction in CO_2-saturated H_2O and 5 %CO_2/Ar-saturated H_2O. Slight morphology deformation was observed after sonolysis in CO_2-saturated H_2O (Fig. 5a-b and Figures S5-S6), whereas the morphology seemed unaltered in 5 %CO_2/Ar-saturated H_2O (Fig. 5c). XRD (Fig. 5d and Figure S7) showed no apparent changes to crystallinity in either experiment. XPS Cu LMM spectra (Fig. 5d) confirmed that Cu^+ species (~569.0 eV) were prevalent in all catalysts (pre and post sonolysis), in line with the crystal phases from the XRD patterns [41]. Further analysis of the XPS Cu 2p region (Fig. 5f) evidences the co-existence of Cu^{2+} (~934.7 eV and 954.9 eV corresponding to Cu $2p_{3/2}$ and Cu $2p_{1/2}$ respectively) and Cu^+ (~932.4 eV in the Cu $2p_{3/2}$ region and 952.4 eV in the Cu $2p_{1/2}$ respectively) species [42], with slight variations of Cu^+/Cu^{2+} ratio after reaction in CO_2-saturated H_2O and 5 %CO_2/Ar--saturated H_2O (Table S1). Specifically, the original Cu^+/Cu^{2+} ratio in as-synthesized Cu_2O cube was 0.35, with only a slight reduction to 0.32 and 0.34 after reaction in CO_2-saturated H_2O and 5 %CO_2/Ar-saturated H_2O, respectively, indicating the structural stability of the Cu_2O cubes catalysts, in good agreement with the XRD and SEM data.

3.5. Proposed sonochemical CO_2 reduction mechanisms

Unveiling the syngas formation pathways over the Cu_2O cube sonocatalyst is of essential importance to further optimize the CO_2 reduction efficiency. CO_2 can be directly reduced on Cu_2O surface to produce CO via $CO_2 \rightarrow O + CO$ as reported [27]. Beyond that, various radicals will be spontaneously generated in the vicinity of the Cu_2O cubes. With respect to H_2 formation, H_2O is initially decomposed via $H_2O \rightarrow HO\bullet + H\bullet$ to produce H• radials, followed by $H\bullet + H\bullet \rightarrow H_2$ to synthesize H_2 [28]. Alternatively, CO_2 can be reduced by the generated H• radials spontaneously to generate CO via $CO_2 + H\bullet \rightarrow CO_2H\bullet + H\bullet \rightarrow H_2O + CO$ [27]. Based on these understandings, a schematic illustration of syngas formation over the Cu_2O cube triggered by ultrasound-formed bubble collapse is proposed and shown in Fig. 6. The enhancement of the effects of cavitation is vital to strengthen CO_2 reduction efficiency. Thus, future studies should explore stable porous Cu_2O catalysts or optimized sonochemical systems. This study shows the first proof-of-concept demonstration of using inexpensive Cu-based catalysts for sonochemical CO_2 reduction, verifying that Cu-based materials are also highly effective catalysts that can be deployed for CO_2 reduction via the electricity-driven green acoustic cavitation methodology.

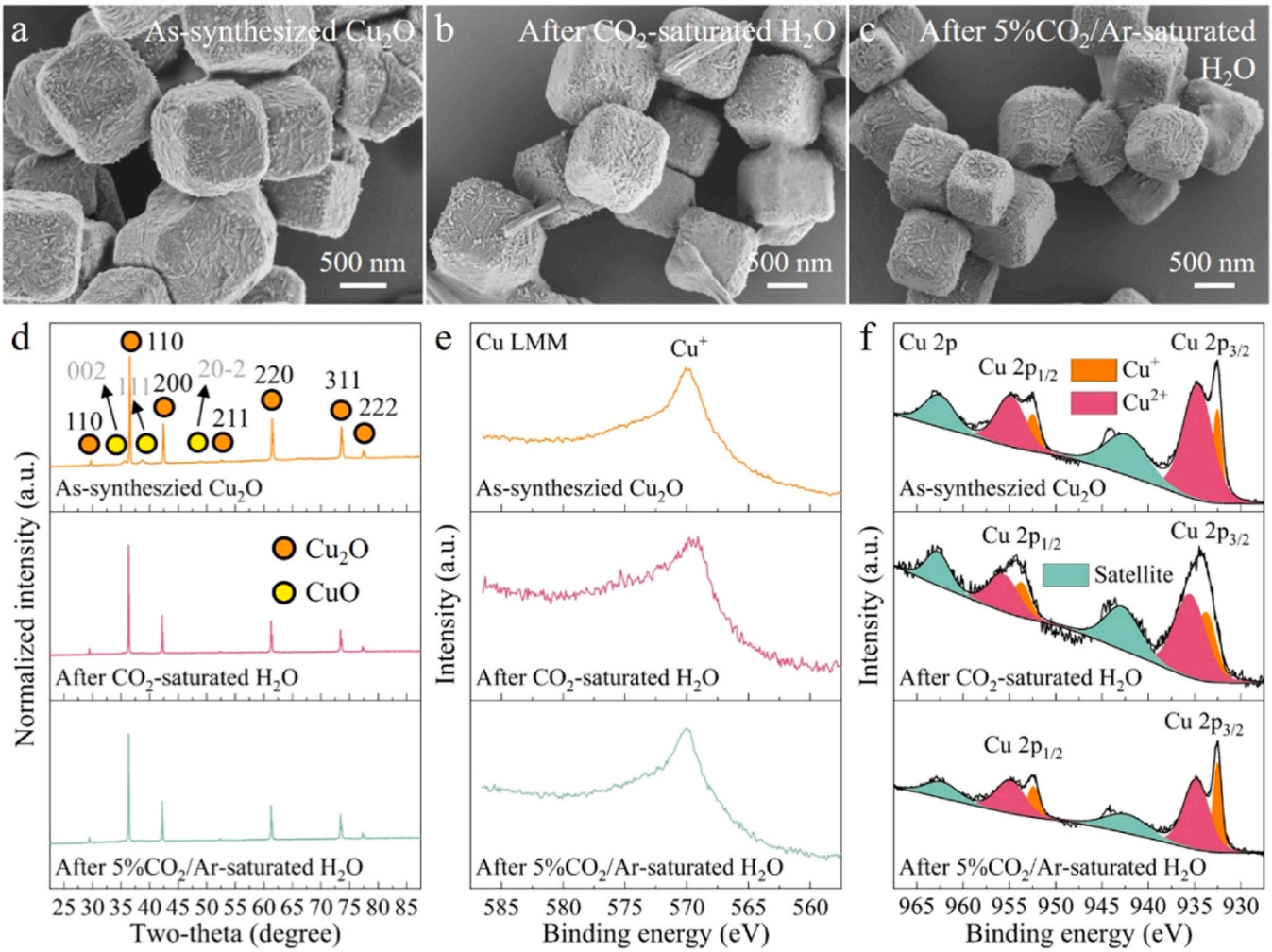

Fig. 5. SEM images of as-synthesized Cu_2O cubes (a), after 20 mins sonochemical CO_2 reduction in CO_2-saturated H_2O (b) and 5 %CO_2/Ar-saturated H_2O (c). XRD patterns (d), XPS Cu LMM spectra (e) and Cu 2p spectra (f) of as-synthesized Cu_2O cubes, after sonochemical CO_2 reduction in CO_2-saturated H_2O and 5 %CO_2/Ar-saturated H_2O.

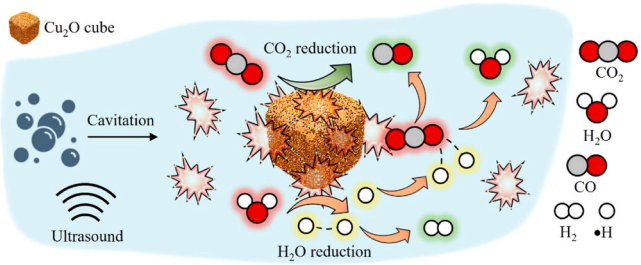

Fig. 6. Schematic demonstration of the proposed sonochemical CO_2 reduction mechanism over Cu_2O cube catalyst to produce syngas, profiling direct CO_2 reduction to CO and H_2O reduction formed H• radicals to reduce CO_2 to CO as well as to form H_2.

4. Conclusions

In this work, four Cu-based catalysts with varied compositions and morphologies were investigated for sonochemical CO_2 reduction. Namely Cu_2O cubes, Cu_7S_4/Cu_2O cubes, Cu_7S_4 cages and Cu_7S_4 sheets catalysts. Furthermore, a range of atmospheres and $KHCO_3$ solutions were systematically explored to assess their sonochemical CO_2 reduction performance towards preferential CO production. All catalysts were shown to be active producing both CO and H_2 under CO_2- and CO_2/Ar-saturated solutions. The CO/H_2 ratio ranged between 1.0 and 2.3 which is within the typical range for syngas. Among the tested catalysts, Cu_2O cubes revealed both the highest activity and stability regarding CO_2 to CO conversion, leading to a marked CO production yield of 272.1 $\mu mol \cdot L^{-1} \cdot g^{-1}$ in CO_2-saturated H_2O. Further measurements in 5 %CO_2/Ar-saturated H_2O significantly enhanced the CO_2-to-CO conversion performance, reaching 1428.8 $\mu mol \cdot L^{-1} \cdot g^{-1}$, equivalent to a CO production rate of 4286.4 $\mu mol \cdot L^{-1} \cdot g^{-1} \cdot h^{-1}$. Interestingly, the less active Cu_7S_4/Cu_2O cubes and Cu_7S_4 cages catalysts were found to have significant structural deformations post testing, while the most active Cu_2O cubes largely retained their structure. Similarly, when the higher performing Cu_2O cube catalysts were assessed in a range of CO_2-saturated $KHCO_3$ solutions, the lowest performing environments were shown to result in the highest structural deformations. This work demonstrates that the inexpensive and scalable Cu-based catalysts have the potential to drive CO_2-to-CO conversion via sonochemistry if further optimizations are carried out to generate materials that retain their structural properties during sonolysis.

CRediT authorship contribution statement

Dong Xia: Writing – review & editing, Writing – original draft, Methodology, Data curation, Conceptualization. **James Kwan:** Writing – review & editing, Supervision, Funding acquisition, Conceptualization. **King Laurie:** Writing – review & editing, Supervision, Resources, Methodology, Funding acquisition, Conceptualization. **Regmi Yagya:** Writing – review & editing, Supervision, Resources, Conceptualization. **Yi Qin:** Writing – review & editing, Methodology, Data curation.

Declaration of Competing Interest

The authors declare that they have no known competing financial interests or personal relationships that could have appeared to influence the work reported in this paper.

Acknowledgements

This work was supported by the UK Catalysis Hub funded by EPSRC grant reference EP/R026645/1. This work was supported by the EPSRC grant reference EP/W012316/1.D. Xia would like to also acknowledge support from the State Key Laboratory of Green and Efficient Development of Phosphorus Resources, Wuhan Institute of Technology.

Appendix A. Supporting information

Supplementary data associated with this article can be found in the online version at doi:10.1016/j.jcou.2025.103220.

Data Availability

Data will be made available on request.

References

[1] A. Jarvis, P.M. Forster, Estimated human-induced warming from a linear temperature and atmospheric CO_2 relationship, Nat. Geosci. 17 (2024) 1222–1224.
[2] M. Mathis, F. Lacroix, S. Hagemann, D.M. Nielsen, T. Ilyina, C. Schrum, Enhanced CO_2 uptake of the coastal ocean is dominated by biological carbon fixation, Nat. Clim. Change 14 (4) (2024) 373–379.
[3] D. Notz, J. Stroeve, Observed Arctic sea-ice loss directly follows anthropogenic CO_2 emission, Science 354 (6313) (2016) 747–750.
[4] S.A. Farooqi, A.S. Farooqi, S. Sajjad, C. Yan, A.B. Victor, Electrochemical reduction of carbon dioxide into valuable chemicals: a review, Environ. Chem. Lett. 21 (3) (2023) 1515–1553.
[5] S. Nitopi, E. Bertheussen, S.B. Scott, et al., Progress and perspectives of electrochemical CO_2 reduction on copper in aqueous electrolyte, Chem. Rev. 119 (12) (2019) 7610–7672.
[6] Y. Wang, L. Qu, H. Ding, P. Webley, G.K. Li, Distributed direct air capture of carbon dioxide by synergistic water harvesting, Nat. Commun. 15 (1) (2024) 9745.
[7] Z. Zhou, T. Ma, H. Zhang, et al., Carbon dioxide capture from open air using covalent organic frameworks, Nature 635 (8037) (2024) 96–101.
[8] J. Wu, S. Ma, J. Sun, et al., A metal-free electrocatalyst for carbon dioxide reduction to multi-carbon hydrocarbons and oxygenates, Nat. Commun. 7 (1) (2016) 13869.
[9] Z. Xie, E. Huang, S. Garg, S. Hwang, P. Liu, J.G. Chen, CO_2 fixation into carbon nanofibres using electrochemical–thermochemical tandem catalysis, Nat. Catal. 7 (1) (2024) 98–109.
[10] P.B. Pati, R. Wang, E. Boutin, et al., Photocathode functionalized with a molecular cobalt catalyst for selective carbon dioxide reduction in water, Nat. Commun. 11 (1) (2020) 3499.
[11] A. Dehane, S. Merouani, A. Chibani, O. Hamdaoui, M. Ashokkumar, Sonochemical and sono-assisted reduction of carbon dioxide: a critical review, Chem. Eng. Process. 179 (2022) 109075.
[12] A.H. Babikir, O. Oloye, K.K. Ostrikov, A.P. O'Mullane, Sonochemical CO_2 reduction to acetamide and liquid C_{2+} oxygenates using a liquid metal Gallium-Based reductant, Chem. Mater. 36 (5) (2024) 2554–2565.
[13] S. Gireesan, A.B. Pandit, Modeling the effect of carbon-dioxide gas on cavitation, Ultrason. Sonochem. 34 (2017) 721–728.
[14] Y. Asakura, K. Yasuda, Frequency and power dependence of the sonochemical reaction, Ultrason. Sonochem. 81 (2021) 105858.
[15] H. Jiao, Q. Mao, N. Razzaq, R. Ankri, J. Cui, Ultrasound technology assisted colloidal nanocrystal synthesis and biomedical applications, Ultrason. Sonochem. 103 (2024) 106798.
[16] M. Li, R. Manica, B. Xiang, Q. Liu, Effect of NaCl and CO_2 on the inception control of hydrodynamic cavitation by gas solubility change, Chem. Eng. Sci. 246 (2021) 116997.
[17] C.C.Y. Wong, J.L. Raymond, L.N. Usadi, et al., Enhancement of sonochemical production of hydroxyl radicals from pulsed cylindrically converging ultrasound waves, Ultrason. Sonochem. 99 (2023) 106559.
[18] V. Mahendran, Q.T. Trinh, X. Zhangyue, et al., Localized oxidative catalytic reactions triggered by cavitation bubbles confinement on copper oxide microstructured particles, Angew. Chem. Int. Ed. 64 (6) (2025) e202416543.
[19] S. Merouani, O. Hamdaoui, S.M. Al-Zahrani, Toward understanding the mechanism of pure CO_2-quenching sonochemical processes, JCTB 95 (3) (2020) 553–566.
[20] J. Rooze, E.V. Rebrov, J.C. Schouten, J.T.F. Keurentjes, Effect of resonance frequency, power input, and saturation gas type on the oxidation efficiency of an ultrasound horn, Ultrason. Sonochem. 18 (1) (2011) 209–215.
[21] Y.Y. Birdja, E. Pérez-Gallent, M.C. Figueiredo, A.J. Göttle, F. Calle-Vallejo, M.T. M. Koper, Advances and challenges in understanding the electrocatalytic conversion of carbon dioxide to fuels, Nat. Energy 4 (9) (2019) 732–745.
[22] J. Wu, Y. Huang, W. Ye, Y. Li, CO_2 reduction: from the electrochemical to photochemical approach, Adv. Sci. 4 (11) (2017) 1700194.
[23] S. Roy, A. Cherevotan, S.C. Peter, Thermochemical CO_2 hydrogenation to single carbon products: scientific and technological challenges, ACS Energy Lett. 3 (8) (2018) 1938–1966.
[24] S. Amanullah, P. Saha, A. Nayek, M.E. Ahmed, A. Dey, Biochemical and artificial pathways for the reduction of carbon dioxide, nitrite and the competing proton reduction: effect of 2nd sphere interactions in catalysis, Chem. Soc. Rev. 50 (6) (2021) 3755–3823.
[25] X. Zhu, H. Xu, C. Bi, et al., Piezo-photocatalysis for efficient charge separation to promote CO_2 photoreduction in nanoclusters, Ultrason. Sonochem. 101 (2023) 106653.

[26] C. Bi, H. Xu, G. Zhou, et al., Lattice energy transfer from homo-crystalline substitution for enhanced piezo-photocatalytic CO_2 conversion, Chem. Eng. J. 501 (2024) 157345.
[27] M.H. Islam, O.S. Burheim, J.-Y. Hihn, B.G. Pollet, Sonochemical conversion of CO_2 into hydrocarbons: the sabatier reaction at ambient conditions, Ultrason. Sonochem. 73 (2021) 105474.
[28] H. Harada, Sonochemical reduction of carbon dioxide, Ultrason. Sonochem. 5 (2) (1998) 73–77.
[29] J. Ma, X. Xiong, C. Ban, K. Wang, J.-Y. Dai, X. Zhou, Ultrasound-triggered sonocatalytic reduction of CO_2 via $H_2Ti_3O_7$ nanowires, Appl. Phys. Lett. 121 (26) (2022) 263901.
[30] L. Chen, Y. Qin, C.T. Coulthard, et al., Catalytic ultrasound-driven synthesis of syngas from CO_2 saturated water, Energy Environ. Sci. 18 (2025) 5389–5396.
[31] Z. Zhang, L. Bian, H. Tian, et al., Tailoring the surface and interface structures of Copper-Based catalysts for electrochemical reduction of CO_2 to ethylene and ethanol, Small 18 (18) (2022) 2107450.
[32] L. Zaza, K. Rossi, R. Buonsanti, Well-defined copper-based nanocatalysts for selective electrochemical reduction of CO_2 to C_2 products, ACS Energy Lett. 7 (4) (2022) 1284–1291.
[33] S. Sun, D. Deng, C. Kong, X. Song, Z. Yang, Twins in polyhedral 26-facet Cu_7S_4 cages: synthesis, characterization and their enhancing photochemical activities, Dalton Trans. 41 (11) (2012) 3214–3222.
[34] B. Gielen, S. Marchal, J. Jordens, L.C.J. Thomassen, L. Braeken, T. Van Gerven, Influence of dissolved gases on sonochemistry and sonoluminescence in a flow reactor, Ultrason. Sonochem. 31 (2016) 463–472.
[35] J.H. Lee, S. Kattel, Z. Jiang, et al., Tuning the activity and selectivity of electroreduction of CO_2 to synthesis gas using bimetallic catalysts, Nat. Commun. 10 (1) (2019) 3724.
[36] H. Chen, Z. Lian, X. Zhao, et al., The role of manganese in CoMnOx catalysts for selective long-chain hydrocarbon production via Fischer-Tropsch synthesis, Nat. Commun. 15 (1) (2024) 10294.
[37] W. Wu, J. Luo, J. Zhao, et al., Facet sensitivity of iron carbides in Fischer-Tropsch synthesis, Nat. Commun. 15 (1) (2024) 6108.
[38] W. Tang, J. Zhu, H. Sun, et al., Study on ultrasound-assisted preparation of sphere-like high-purity alumina, J. Alloy Compd. 966 (2023) 171500.
[39] K. Kerboua, O. Hamdaoui, Energetic challenges and sonochemistry: a new alternative for hydrogen production? Curr. Opin. Green. Sustain. Chem. 18 (2019) 84–89.
[40] M.H. Islam, O.S. Burheim, B.G. Pollet, Sonochemical and sonoelectrochemical production of hydrogen, Ultrason. Sonochem. 51 (2019) 533–555.
[41] G. Ma, O.A. Syzgantseva, Y. Huang, et al., A hydrophobic Cu/Cu_2O sheet catalyst for selective electroreduction of CO to ethanol, Nat. Commun. 14 (1) (2023) 501.
[42] X. Lv, Y. Tian, F. Wu, et al., Chiral plasmonic-dielectric coupling enables strong near-infrared chiroptical responses from helicoidal core-shell nanoparticles, Nat. Commun. 15 (1) (2024) 9234.